Thin Solid Films 571 (2014) 316–320

Contents lists available at ScienceDirect

Thin Solid Films

journal homepage: www.elsevier.com/locate/tsf

Influence of the IR-mirror layer composition in the mechanical properties of solar selective coatings made from Mo:Si_3N_4 cermet

L. Álvarez-Fraga [a], M.A. Monclús [b], J.M. Molina-Aldareguía [b], J.A. Sánchez-García [a,1], E. Céspedes [a,2], R. Escobar-Galindo [a], C. Prieto [a,*]

[a] Instituto de Ciencia de Materiales de Madrid, CSIC, Cantoblanco, 28049 Madrid, Spain
[b] IMDEA Materials Institute, C/Eric Kandel 2, 28906 Getafe, Madrid, Spain

ARTICLE INFO

Available online 9 June 2014

Keywords:
Solar selective coatings
IR-mirror layers
mechanical properties of CSP coatings

ABSTRACT

Solar selective coating multilayers deposited by magnetron sputtering and containing Mo:Si_3N_4 cermet as the absorber layer and Ag as infrared reflector (IR-mirror) have shown excellent optical characteristics for concentrated solar power applications at high temperatures. However, mechanical reliability of such optical coatings is a concern due to the large thermal mismatch between the Mo:Si_3N_4 cermet and the Ag IR-mirror layer. The substitution of the Ag IR-mirror layer by a Ti/Ag bilayer can improve mechanical reliability at the operating conditions, but at the expense of deteriorating the optical properties of the solar selective coating. In this work, we study the evolution of the mechanical and optical properties of Mo:Si_3N_4/Ti/Ag solar selective coatings, as a function of the Ti/Ag ratio, with the objective of finding a compromise between the optical and mechanical properties. The substitution of Ag by Ti improves the multilayers scratch resistance without deteriorating the optical properties. As a result, we suggest an optimal composition of the Ti/Ag IR-mirror bilayer.

1. Introduction

Thermo-solar conversion is one of the simplest methods of sustainable energy production. In this direct heating technology, solar energy efficiency is essentially determined by the solar selective coatings, requiring high solar absorbance and low thermal emittance, with the solar absorber material being of fundamental importance. Since the efficiency of concentrated solar power system increases with operating temperature, research has been aimed at designing selective solar coatings with optimum optical properties at high temperatures (>400 °C) [1]. For this purpose, the fabrication of coatings by physical vapor deposition has become one of the most promising technologies. Currently, most of the commercial solar selective coatings (SSC) are prepared by magnetron sputtering [2], which is a dry, clean and eco-friendly technology. This deposition technique allows large area deposition with very precise control of layer composition and thickness (down to nanometer scale), which is the key to accomplish the required optical absorbance of the solar selective coating.

Among the different strategies to optimize the required spectral selectivity, the design of multilayer coatings is of special interest because of their high solar efficiency at medium and high temperatures. In this sense, the design that has proven to give higher solar performances [3–5] is formed by four layers: (i) a buried infrared reflective metallic layer (IR-mirror), (ii) a high metal volume fraction (HMVF) cermet layer, (iii) a low metal volume fraction (LMVF) cermet layer, and (iv) a top anti-reflective (AR) layer. Due to the gradual variation of refractive index, a coating with this structure displays very efficient solar radiation absorption due to its internal optical extinction and to the phase interference between the double cermet and the AR layers.

For high temperature applications, however, solar selective stacks generally degrade, causing a decrease in the solar selectivity. In this sense, only a few combinations of materials are suitable for working at temperatures higher than ~400 °C. Among them, Mo-Al_2O_3 and W-Al_2O_3 cermets [6] are stable in the 350–500 °C temperature range and Mo-SiO_2 cermets have been reported to be stable in vacuum conditions up to 580 °C [5]. More recently, nitride tandem systems, as NbAlN/NbAlON [7] and, HfMoN/HfON [8] have been also proposed for high temperature applications. In this work, we have studied multilayer coating based on Mo-Si_3N_4 cermets, which have been shown to be suitable for temperature higher than 600 °C in an earlier study [9]. In that work, the layer thickness and composition of each layer were optimized to obtain an excellent selectivity (defined as the absorptivity to emissivity ratio) for temperatures of 600 °C by using a multilayered structure comprised by the following four layers: an Ag IR-mirror, an absorber bi-layer of Mo-Si_3N_4 cermets and an antireflective film of Si_3N_4. However, mechanical reliability was considered to be an issue due to the large thermal mismatch between the Mo-Si_3N_4 cermet and the Ag IR-mirror.

In the present work, we report on the effect of modifying the composition of the IR-mirror layer, by the substitution of the Ag layer by a Ti/Ag

* Corresponding author.
E-mail address: cprieto@icmm.csic.es (C. Prieto).
[1] Present address: TECNALIA, Parque Tecnológico de San Sebastián, Mikeletegi Pasealekua, 2, E-20009 San Sebastián, Gipuzkoa, Spain.
[2] Present address: Institute for Science and Technology in Medicine, Keele University, Guy Hilton Research Centre, Thornburrow Drive, Hartshill, Stoke-on-Trent ST4-7QB, UK.

http://dx.doi.org/10.1016/j.tsf.2014.05.069
0040-6090/

bilayer, with the objective of improving the mechanical reliability without compromising the optical properties. In particular, the present work addresses the impact of the Ti/Ag ratio on the optical and adhesion properties of selective solar coatings deposited on stainless steel by sputtering.

2. Experimental

The tandem absorbers were deposited using magnetron sputtering at room temperature on annealed stainless steel AISI-321 substrates (labeled as SSth). After cleaning with acetone and isopropyl alcohol, the stainless steel substrates were annealed at 600 °C in air to develop a thermally grown oxide (TGO) antidiffusion layer. The materials deposited to form the studied stacks were, starting from the substrate side: a Ti/Ag bilayer as metallic IR reflector, two Mo:Si_3N_4 composites as cermet layers, and Si_3N_4 as the top AR layer. The base pressure was around 8.5×10^{-4} Pa. The Ti/Ag bilayer was deposited by direct current (DC) sequential sputtering of Ag and Ti with an Ar pressure of 5×10^{-1} Pa and a target power of 15 W. This metallic IR-layer was subjected to a passivation process prior to deposition of the next layers. The sample in which the IR-mirror layer is formed only by Ag, its surface was passivated by flowing oxygen to achieve a chamber pressure of 2 Pa at the chamber, during 10 min. On the other hand, a very thin TiN layer has been used for the rest of the samples. TiN was deposited by N_2-reactive sputtering of Ti at 7.5×10^{-1} Pa and a DC power of 15 W. As reported elsewhere [9], Mo:Si_3N_4 cermets were prepared by simultaneous co-sputtering of Si and Mo targets using N_2 as reactive gas at 7.5×10^{-1} Pa. Radio-frequency (RF) and DC sputtering were used for Si and Mo, respectively. The metal volume fraction, or filling factors (FF), were modified by tuning the power supplied to each target. Finally, the Si_3N_4 AR layer was prepared by RF sputtering of Si with N_2 at 7.5×10^{-1} Pa and 100 W.

UV–vis-IR reflectance measurements were performed using a Shimadzu SolidSpec-3700 spectrophotometer in the range of 240–2600 nm and a Varian 660-IR spectrometer in the 2.5–25 μm wavelength range. $BaSO_4$ was used as standard reflector in the 240–800 nm range and gold in the whole IR range from 740 nm to 25 μm.

Nanoindentation test was performed with a Hysitron TI950 Triboindenter Instrument equipped with a Berkovich diamond indenter tip using a maximum load of 10 mN, with loading, holding, unloading times of 5 s, 2 s and 5 s respectively. Hardness and modulus at each load were evaluated from the indentation curves using the Oliver and Pharr method [10]. The same instrument, equipped with a transducer with normal (Z-axis) and lateral (Y-axis) force sensors, was used to carry out scratch tests. In this transducer, the load is applied electrostatically and force and displacement are measured capacitively in both the Z and Y-axis using two sensors mounted on opposite sides of the normal transducer at a 90° angle. The load resolutions of the normal and lateral force sensors were 1 nN and 3 nN, respectively. A 10 μm-radius conical diamond tip was used in the scratch experiments. In order to determine the friction coefficient, constant normal force scratches at a force of 500 μN (which did not leave any permanent deformation) were performed at room temperature on each sample. For measuring the scratch resistance, 10 μm-long scratches were carried out, while the normal force (F_N) was ramped and the lateral force (F_L) was simultaneously recorded. The tip was dragged at a velocity of 0.25 μm/s, while the normal force was ramped up to 6 mN. The measured (F_L) signal allows the determination of the critical loads that indicate failure of the top layers, which are detected by sudden increases in the lateral force. A second tip was also used to perform high temperature scratch tests. The high temperature tip was a conical diamond tip with a radius of 10 μm, brazed to a Macor shaft attached directly to the load transducer behind a heat shield, to minimize drift effects during the scratch tests.

All samples were scratched at room temperature, while the high temperature tests at 300 °C were only carried out in the three samples that have shown the most promising room temperature behavior. In all these experiments, at least 10 scratches were carried out and subsequently observed under scanning electron microscopy with a FE-SEM FEI Nova NANOSEM 230, in order to observe the failure events.

3. Results and discussion

The mechanical properties of the four-layer SSC described above are mostly influenced by the interaction between the top ceramic film (absorber cermet and AR layer) and the bottom metallic IR mirror. Si_3N_4 is extremely hard [11], which may be obtained in thin film only when prepared with very low oxygen content [12], and the reliability of the SSC is typically controlled by the metallic IR mirror (for instance, delamination has been observed during vacuum annealing for silver layers thicker than 0.6 μm). In our previous investigation [9], an Ag IR-mirror layer with thickness ~80 nm was found to be optimum with respect to the optical properties. In the present work, we investigate the impact of the partial substitution of Ag by Ti to improve the mechanical behavior, without compromising the optical properties. To this end, a series of SSC stacks were prepared by maintaining a constant IR-mirror layer thickness (60–70 nm), in which the gradual substitution of the Ag layer by a Ti/Ag bilayer with increasing content of Ti. Table 1 summarizes the multilayer structure of the studied selective coatings, where the labels indicate the Ti volume fraction (VF) defined as the ratio between the Ti layer and the total Ti/Ag bilayer thicknesses.

3.1. Optical properties

Fig. 1(a) plots the reflectivity of the full set of selective coatings under study. First, the impact of the 10 nm thick TiN film used to passivate the Ti interface was studied, by determining the influence of adding a TiN layer on top of the Ag layer (sample SAg80 vs. SAgTiN). The low/high reflectivity transition shows a shift to higher wavelengths when a TiN passivation layer is present, as shown in Fig. 1(a). This is an interference effect that could be easily minimized by a slight variation of the cermet layer thickness.

The partial substitution of Ag by Ti induces a shift of the characteristic wavelength for the low/high reflectivity transition, as observed in Fig. 1(a) between sample SAgTiN (with 0% Ti-VF) and sample STi71 (with 71% Ti-VF). Up to this point (71% Ti-VF), the reflectivity spectra present the same degree of abruptness between their low and high regions. This is the important feature that determines selectivity between

Table 1
Multilayer structure (layer thickness, Ti volume fraction and cermet filling factors) of the studied stacks. The corresponding solar absorptivity (αsol) and thermal emissivity (εth) (at 25 °C and 450 °C) was calculated in the 0.25−4 μm and 0 – 30 μm ranges, respectively, from the experimentally measured reflectivity by using the AM1.5 solar spectrum and the blackbody emission curve.

Sample	Ag thick. (nm)	Ti thick. (nm)	Ti-VF Ti/(Ti + Ag) (%)	TiN thick. (nm)	Mo-Si_3N_4 (HMVF)		Mo-Si_3N_4 (LMVF)		Si_3N_4 AR-layer thick. (nm)	α_{Sol}	$\varepsilon_{25\,°C}$	$\varepsilon_{450\,°C}$
					FF (%)	Thick. (nm)	FF (%)	Thick. (nm)				
SAg80	80	0	0	0	37	50	20	55	60	0.91	0.010	0.071
SAgTiN	60	0	0	11	37	50	20	55	60	0.89	0.039	0.108
STi14	60	10	14	11	37	50	20	55	60	0.877	0.034	0.122
STi43	40	30	43	11	37	50	20	55	60	0.906	0.035	0.171
STi71	20	50	71	11	37	50	20	55	60	0.923	0.063	0.251
STi100	0	70	100	11	37	50	20	55	60	0.936	0.195	0.506

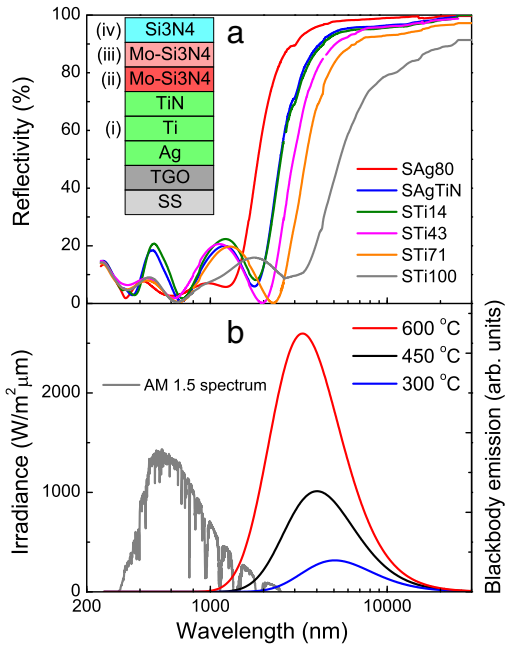

Fig. 1. (a) Reflectivity spectra of selective coating stacks based on Ag/Ti/Mo-Si_3N_4 (HMVF)/Mo-Si_3N_4 (LMVF)/Si_3N_4. Inset shows a schematic view of the stacks. (b) The standard ASTM AM1.5D solar spectrum received at the earth surface and the black-body emission Planck function at different temperatures are given for appraisal of the above reflectivity spectra.

visible and infrared wavelengths, while its position may be tuned with an appropriate/another selection of thickness and metal volume fraction of the cermet layers. On the contrary, the sample with a 100% Ti-VF in the IR mirror, shows a reduced reflectivity, because Ti is not as good IR reflector as silver.

Using the experimentally obtained spectral reflectance data $R(\lambda)$, the solar-weighted absorptivity α_{Sol} reported in Table 1 can be calculated from [6]:

$$\alpha_{Sol} = \frac{\int_{\lambda_1}^{\lambda_2} [1-R(\lambda)]A(\lambda)d\lambda}{\int_{\lambda_1}^{\lambda_2} A(\lambda)d\lambda} \quad (1)$$

where $A(\lambda)$ is the ASTM AM1.5D solar spectral irradiance [13] (showed in Fig. 1(b)). α_{Sol} has been calculated with integration limits $\lambda_1 = 0.25$ μm and $\lambda_2 = 2.5$ μm to account for the whole solar spectrum.

On the other hand, the thermal emissivity ε_{th} at a specific temperature T is determined by using [6]:

$$\varepsilon_{th}(T) = \frac{\int_0^{\infty} L(T,\lambda)[1-R(\lambda)]d\lambda}{\int_0^{\infty} L(T,\lambda)d\lambda} \quad (2)$$

where $L(T, \lambda)$ is the black body emission Planck function at the required temperature, as shown in Fig. 1(b) for three representative temperatures. Even though the spectral reflectance, and consequently the absorptivity and emissivity, is also directionally dependent ($R(\lambda, \theta)$), the measured near normal spectral reflectance ($R(\lambda)$) provides a good approximation. This method to compute the thermal emissivity at high temperatures is based on the assumption that the reflectance spectrum is constant with temperature and its temperature dependence is only given by entering the corresponding Planck function in Eq. (2). We have performed integration up to 30 μm to take into account the full range where the black body radiation may be appreciable. Consequently, since reflectivity spectra are essentially constant at high wavelengths,

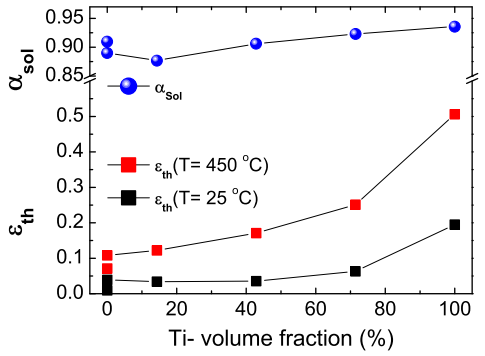

Fig. 2. Solar absorptivity (α_{sol}) and thermal emissivity (ε_{th}) at 25 °C and 450 °C vs. the Ti-volume fraction defined as the metal layer thickness ratio forming the IR-mirror .

$R(\lambda)$ has been extrapolated between 25 and 30 μm as equal to the last measured value. It should be commented that, recently, we have validated this method of evaluating the thermal emissivity by performing measurements of the spectral emissivity [14] at several temperatures to obtain the temperature behavior of the thermal emissivity in similar selective coatings. Table 1 summarizes the emissivity values obtained using Eq. (2) (with integration from 1 to 30 μm) evaluated at $T = 25$ °C and $T = 450$ °C, for each studied SSC.

Fig. 2 shows the evolution of the obtained α_{sol} and ε_{th} as a function of the titanium volume fraction in the IR-mirror layer. The obtained values of solar absorptivity did not show any significant variations along the series, but the thermal emissivity increased with the Ti volume fraction in the IR-mirror. This trend was even more noticeable at 450 °C because it is caused by the observed shift of the reflectivity spectra. In any case, the reflectivity of the "STi100 coating" was completely different to the rest, due to the different nature of Ti IR-mirror (without silver), which provides a significant increase of ε_{th}. It should be noted that results were not modified after repeated vacuum annealing at temperatures below 600 °C for several periods of 15 h, corroborating the thermal stability of the selective coatings. Therefore, it was concluded that the

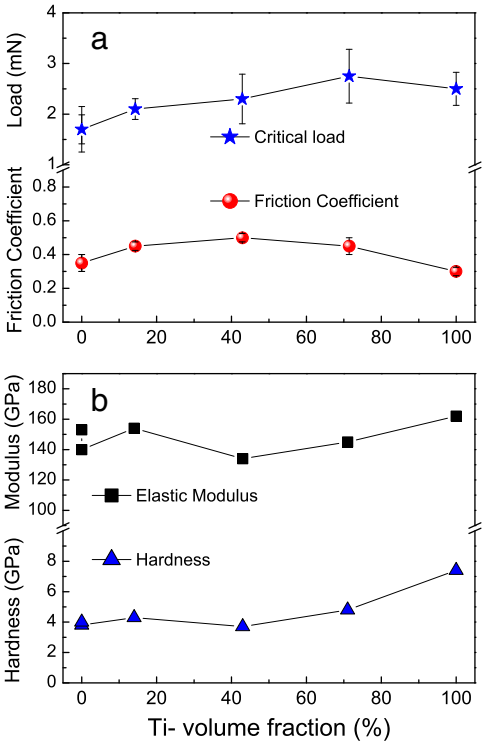

Fig. 3. (a) Critical load and friction coefficient of selective coating stacks vs. the Ti-volume fraction in the IR-mirror. (b) Elastic modulus and hardness.

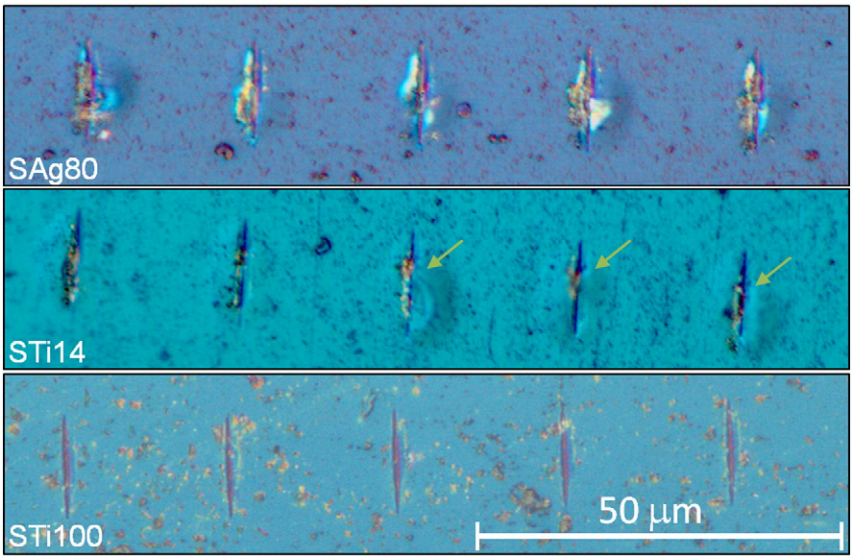

Fig. 4. Optical images of scratches performed on samples SAg80, STi14 and STi100 using a ramp force applied during 40 s until a maximum load of 6 mN was reached.

partial substitution of Ag by Ti in the IR-mirror layer did not substantially modify the required optical properties of the SSC.

3.2. Mechanical properties

Nanoscratch experiments were performed on all samples to evaluate the influence of the Ti addition to the adhesion of the coatings. We found that the thin TiN passivation layer had no influence on the critical load or on the friction coefficient. Fig. 3(a) shows the variation of the critical load and friction coefficient as a function of Ti-VF in the IR-mirror bilayer. Critical loads usually indicate the start of failure events along the scratch length. The results showed the critical load increase with the Ti-VF, with values ranging from ≈1.7 mN for 0% to ≈2.8 mN for 100% Ti content. The friction coefficient ranged between 0.3 and 0.5, peaking for a Ti-VF of 43%.

Fig. 4 shows optical microscope images of the scratches corresponding to samples SAg80, STi14 and STi100. For the sample with only Ag in the IR-mirror (SAg80), the scratch caused gross delamination almost from the beginning, resulting in the lower critical loads found in this case (Fig. 3(a)). For sample STi14, some cracks and lift off of the top layer were observed (pointed by arrows), whereas for STi100, the deformation behavior was more ductile.

High resolution scanning electron microscopy (HR-SEM) was used to observe the failure events on selected scratches in samples STi14 and STi100 (Fig. 5). In general, stacks containing Ag in the IR-mirror layer showed cracks and coating delamination extending in some cases well away from the scratch track, as seen in Fig. 5(a) and (b). With further increase in the normal load, the perforation of the top cermet layers occurred, with the eventual lift off of the Ag layer. On the contrary, the deformation behavior of stacks containing only Ti in the IR-mirror layer (sample STi100) was more ductile (Fig. 5(c) and (d)). The SEM images show discontinuous ductile perforation of the top layers combined with the appearance of small transversal cracks signaling the onset of the critical load. It is important to notice that this change in failure mode to less gross delamination occurred as soon as Ti was introduced in the IR-mirror, even for the lowest Ti-VF of 14%, even though the impact of the Ti-VF on the determined critical loads was only marginal.

High temperature scratches performed on three of the samples at $T = 300$ °C resulted in a more ductile deformation compared with scratches performed at room temperature. The critical loads measured at 300 °C were higher than that at room temperature with no evidence of cracks on the wear track. Average critical loads were ≈8.5 mN for sample STi14 (14% Ti-VF) and ≈5 mN for samples SAg80 and SAgTiN (0% Ti-VF). This finding corroborates the beneficial effects that the partial substitution of Ag by Ti in the IR-mirror has on the scratch resistance of the SSCs.

Additionally, Fig. 3(b) shows the indentation hardness and elastic modulus results obtained at a load of 10 mN, which resulted in a penetration depth of ≈200 nm. Indentations at lower loads resulted in a

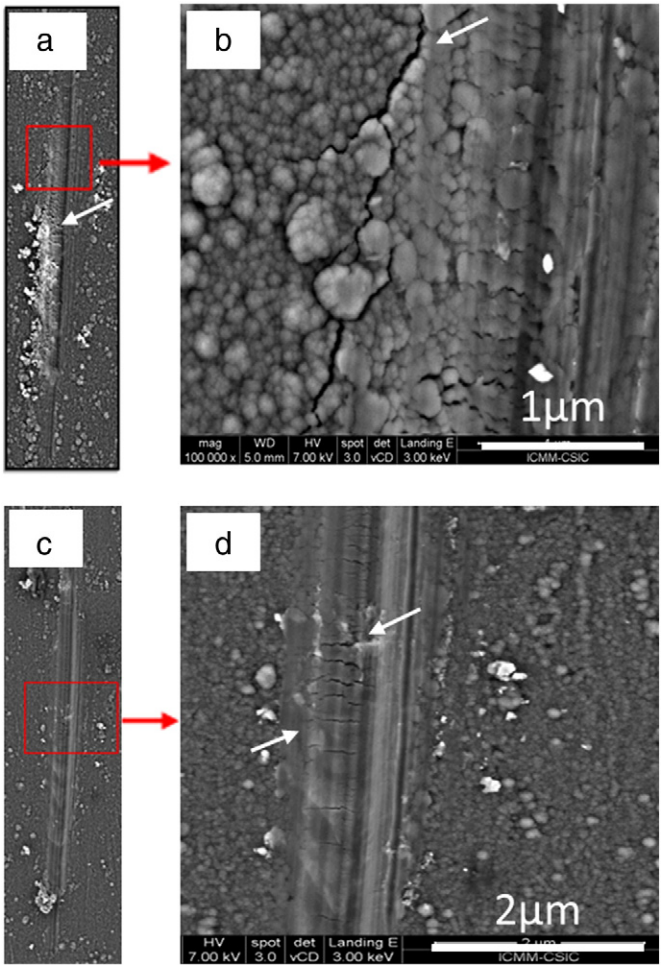

Fig. 5. SEM images of scratches of two representative samples. (a) and (b) STi14 stack. (c) and (d) STi100 stack. Arrows point at clustered failure events which correspond to critical loads of ~2.1 mN (STi14) and ~2.5 mN (STi100). The maximum applied load was 6 mN.

large scatter in the data, due to the roughness (R_a) of the coatings, which ranged from ≈20 nm to ≈40 nm. Therefore, in order to avoid tip rounding and roughness effects on the measured properties, only values obtained at loads of 10 mN are reported. Since the indentation depth is larger than the total coating thickness (≈150 nm), the hardness and modulus values reflect the combined response of the coating and the steel substrate. The introduction of Ti in the IR-mirror resulted in negligible effects in both hardness and modulus for Ti-VF <50%, with hardness values in the range between ≈4.0 GPa and ≈4.4 GPa and elastic modulus of the order of 150 GPa. However, increasing the Ti-VF beyond 50% caused an increase in hardness, reaching ≈5.6 GPa for 100% Ti-VF.

In summary, the substitution of Ag IR-mirror layer, by a Ti/Ag bilayer, increased the scratch resistance of the selective coatings: the critical load for the onset of coating failure increased and the deformation mode change from gross delamination to a more ductile behavior. The improvement in adhesion was noticeable already with a Ti-VF of 14%, while the presence of Ti, up to a Ti-VF of 71%, does not have a detrimental effect in the optical properties of the selective coatings (Fig. 2). However, the complete substitution of the Ag IR-mirror layer by Ti degraded the optical properties of the coatings. Therefore, for the range of samples investigated, the STi14 coating, with a Ti-VF of 14%, appears to offer the best compromise between mechanical and optical properties since more Ti does not improve the mechanical properties in a significant manner, whereas the optical properties remain at an optimum level.

4. Conclusions

Solar selective coating multilayers, based on a Ti/Ag bimetallic layer as the IR-mirror, a double Mo:Si_3N_4 cermet layer as the absorber and a top Si_3N_4 antireflective layer, have been prepared by sputtering. A SSC set in which the Ti/Ag fraction is varied was optically and mechanically characterized to find the best compromise between the optical and the mechanical integrity of the coating. It was found that using a Ti/Ag IR-mirror bilayer, with a Ti-VF between 17% and 71% did not degrade the optical properties, but significantly improved scratch resistance of the coatings. This study demonstrates that, by a careful design of the IR-mirror layer, it is possible to improve the mechanical integrity of selective solar coating, without degradation of their optical performance.

References

[1] C.E. Kennedy, Review of Mid- to High-Temperature Solar Selective Absorber Materials, NREL/TP-520-31267, National Renewable Energy Laboratory, July 2002.
[2] N. Selvakumar, H.C. Barshilia, Review of physical vapor deposited (PVD) spectrally selective coatings for mid- to high-temperature solar thermal applications, Sol. Energy Mater. Sol. Cells 98 (2012) 1.
[3] Q.-C. Zhang, D.R. Mills, High solar performance selective surface using bi-sublayer cermet film structures, Sol. Energy Mater. Sol. Cells 27 (1992) 273.
[4] Y. Yin, R.E. Collins, Optimization and analysis of solar selective surfaces with continuous and multilayer profiles, J. Appl. Phys. 77 (1995) 6485.
[5] S. Esposito, A. Antonaia, M.L. Addonizio, S. Aprea, Fabrication and optimization of highly efficient cermet-based spectrally selective coatings for high temperature, Thin Solid Films 517 (2009) 6000.
[6] Q.-C. Zhang, Y. Yin, D.R. Mills, High efficiency Mo-Al_2O_3 cermet selective surfaces for high-temperature application, Sol. Energy Mater. Sol. Cells 40 (1996) 43.
[7] H.C. Barshilia, Spectrally selective NbAlN/NbAlON/Si_3N_4 tandem absorber for high-temperature solar applications, Sol. Energy Mater. Sol. Cells 92 (2008) 495.
[8] N. Selvakumar, N.T. Manikandanath, A. Biswas, H.C. Barshilia, Design and fabrication of highly thermally stable HfMoN/HfON/Al_2O_3 tandem absorber for solar thermal power generation applications, Sol. Energy Mater. Sol. Cells 102 (2012) 86.
[9] E. Céspedes, M. Wirz, J.A. Sánchez-García, L. Álvarez-Fraga, R. Escobar-Galindo, C. Prieto, Novel Mo-Si_3N_4 based selective coating for high temperature concentrating solar power applications, Sol. Energy Mater. Sol. Cells 122 (2014) 217.
[10] W.C. Oliver, G.M. Pharr, An improved technique for determining hardness and elastic modulus using load and displacement sensing indentation experiments, J. Mater. Res. 7 (1992) 1564.
[11] P. Walsh, A. Omeltchenko, R.K. Kalia, A. Nakano, P. Vashishta, S. Saini, Nanoindentation of silicon nitride: a multimillion-atom molecular dynamics study, Appl. Phys. Lett. 82 (2003) 118.
[12] M. Vila, D. Cáceres, C. Prieto, Mechanical properties of sputtered silicon nitride thin films, J. Appl. Phys. 94 (2003) 7868.
[13] http://rredc.nrel.gov/solar/spectra/am1.5 (accessed: May 2013).
[14] I. Setién-Fernández, T. Echániz-Ariceta, L. González-Fernández, R.B. Pérez-Sáez, E. Céspedes, J.A. Sánchez-García, L. Álvarez-Fraga, R. Escobar-Galindo, J.M. Albella, C. Prieto, M.J. Tello, First spectral emissivity study of a solar selective coating in the 150–600 °C temperature range, Sol. Energy Mater. Sol. Cells 117 (2013) 390.